The Cell Surface 1 (2018) 25–33

Contents lists available at ScienceDirect

The Cell Surface

journal homepage: www.journals.elsevier.com/the-cell-surface

Intermolecular interactions between glycomodules of plant cell wall arabinogalactan-proteins and extensins

Li Tan[a,*,1], David Tees[b], Jin Qian[a,1], Sulaiman Kareem[b,2], Marcia J. Kieliszewski[a]

[a] Department of Chemistry and Biochemistry, Ohio University, Athens, OH 45701, USA
[b] Department of Physics and Astronomy, Ohio University, Athens, OH 45701, USA

ARTICLE INFO

Keywords:
Arabinogalactan-proteins
Extensins
Hydroxyproline-rich glycoproteins
Wall ions
Intermolecular interaction
Forced unbinding microscopy

ABSTRACT

Hydroxyproline-rich glycoproteins (HRGPs) are a unique component of plant cell walls, undergoing extensive posttranslational modification such as proline hydroxylation and hydroxyproline-O-glycosylation. Arabinogalactan proteins (AGPs) and extensins are major members of the HRGP superfamily. AGPs have repetitive AlaHyp, SerHyp, and ThrHyp peptides, the Hyp residues being glycosylated with large type II arabinogalactan polysaccharides, while extensins contain characteristic $SerHyp_4$ and $SerHyp_2$ motifs with arabinosylated (1–4 residues) Hyp. Although they are less than ten percent in all wall materials, AGPs and extensins play important roles in all aspects of plant growth and development. The detailed mechanisms of their functions are still under investigation. However, many of the functions may be attributed to their adhesive properties. Here, we used a forced unbinding technique to measure relative adhesive potential of the well characterized $(AlaHyp)_{51}$ and $(SerHyp_4)_{18}$ glycomodules representing AGPs and extensins, respectively. In the presence of different wall ions such as protons, Ca^{2+}, and boron, the glycomodules exhibited different adhesive patterns, suggesting that the wall ion-regulated intermolecular interactions/adhesions between AGPs and/or extensins may be involved in maintaining wall-plasma membrane integrity during wall loosening processes such as wall elongation or expansion. This research applies a biophysical approach to understand the biological function of plant cell wall glycoproteins.

Introduction

The plant cell wall is a dynamic matrix composed of cellulose, hemicelluloses, pectins, enzymes, and structural proteins, including hydroxyproline-rich glycoproteins (HRGPs). Like collagens of the animal extracellular matrix, HRGPs serve as an important scaffolding component of the plant extracellular matrix, which is composed of apoplast and cell wall. HRGPs can be classified into three subfamilies, including the highly glycosylated arabinogalactan-proteins (AGPs), the moderately glycosylated extensins, and the least glycosylated proline-rich proteins (PRPs) (Kieliszewski et al., 2010). In the HRGP superfamily, AGPs possess different clustered glycosylation motifs such as AlaHyp, SerHyp, and ThrHyp in the polypeptide backbones, the Hyp residues heavily glycosylated with type II arabinogalactan (AG) polysaccharides that account up to 95% of the molecular weight. In contrast, extensins share characteristic $SerHyp_4$ glycosylation motifs in which each Hyp residue is decorated with oligoarabinosides. Using a synthetic gene approach, repetitive glycomodules $(AlaHyp)_{51}$ and $(SerHyp_4)_{18}$ were produced in suspension cultured transgenic tobacco cells (Tan et al., 2003; Shpak et al., 2001). All the Hyp residues in the $(AlaHyp)_{51}$ glycomodules were glycosylated with arabinogalactan polysaccharides, while all the Hyp residues in the $(SerHyp_4)_{18}$ glycomodules were substituted with short arabinosides, consistent with the Hyp-contiguity hypothesis (Kieliszewski, 2001). Thus, these two glycomodules represent the glycosylated regions of typical AGPs and extensins, respectively.

AGs in endogenous AGPs bear up to 120 sugar residues per polysaccharide (Ellis et al., 2010). With the emergence of new technologies, we now have detailed analyses of AG structures (Gane et al., 1995; Tan et al., 2004, 2010; Tryfona et al., 2010, 2012). Although various structural elements were identified from AGP samples isolated from different plant materials, the well characterized type II AGs generally contain 1–3 linked β-Gal backbones with 6-linked β-Gal side-chains that are decorated with Ara, GlcA, Rha, and/or Fuc residues (Ellis et al., 2010; Tan et al., 2012). The extensin arabinosides, including $Hyp\text{-}Ara_4$, $Hyp\text{-}Ara_3$, $Hyp\text{-}Ara_2$, and Hyp-Ara, consist of β-Ara*f* residues, except

* Corresponding author.
E-mail address: tan@ccrc.uga.edu (L. Tan).
[1] Present address: Complex Carbohydrate Research Center, University of Georgia, 315 Riverbend Road, Athens, GA 30602, USA.
[2] Present address: Stephen M. Ross School of Business, University of Michigan, 701 Tappan St., Ann Arbor, MI 48109, USA.

https://doi.org/10.1016/j.tcsw.2018.03.001
Received 7 February 2018; Received in revised form 27 February 2018; Accepted 1 March 2018
Available online 22 March 2018
2468-2330/ Published by Elsevier B.V.

that the terminal Ara residues of Hyp-Ara_4 are α-linked (Akiyama et al., 1980; Chen et al., 2015). Because AGPs usually contain negatively charged GlcA residues and extensins are Lys-rich, and therefore positively charged, AGPs and extensin monomers are believed to be incorporated into cell walls by ionic forces, being released on application of salt solutions (Serpe and Nothnagel, 1995; Cannon et al., 2008). In addition, the hydroxyl groups of their sugar moieties are undoubtedly involved in H-bonding with other wall components (Seifert and Roberts, 2007).

AGPs and extensins are involved in many aspects of plant growth and development (Seifert and Roberts, 2007; Lamport et al., 2011). For the more lightly glycosylated extensins, biological functions may depend on the properties of both the exposed polypeptide regions as well as the attached oligoarabinosides (Cannon et al., 2008). For example, the alignment of the extensin cross-linking motifs in the polypeptides of AtEXT3 (or RSH) monomers results in formation of network structure in vitro (Cannon et al., 2008). Although the protein portions of chimeric AGPs such as the two adhesive fasciclin-like domains in the Arabidopsis SOS5 (AtFLA4) protein are believed to contribute to function in vivo (Shi et al., 2003; Schultz et al., 2000), it is likely that the peripheral carbohydrate moieties play a central role in AGP functions as AG polysaccharides are the predominant components of all "classic" AGPs (Seifert and Roberts, 2007; Ellis et al., 2010; Tan et al., 2012). AG peptides that have only 10–15 amino acid residues but possess large AG polysaccharides are extreme examples of the prominent role of AG polysaccharides in AGP structure and hence function (Schultz et al., 2004). Undoubtedly the functions of AGPs and extensins reside in their interactions with each other and with other wall components (Seymour et al., 2004), including wall polysaccharides, signaling molecules and possibly receptors on plasma membranes (Seifert and Roberts, 2007; Ellis et al., 2010; Coimbra and Pereira, 2012), however, the detailed mechanisms of such intermolecular interactions remain unknown.

Here we used a forced unbinding technique (Tees et al., 2001) to evaluate the adhesion properties of AGPs and extensins in vitro. Forced unbinding is a class of techniques that can directly probe and manipulate receptor-ligand bonds. There are several modes that can be used for assessing bonding. In the most labor-intensive force spectroscopy methods, the distribution of forces as a function of bond loading rate is measured and the results are used to determine the force dependence of the bond unbinding rate, which is related to the energy landscape of the bonds (Merkel et al., 1999; Tees et al., 2001b; Arya et al., 2005). Alternatively, adhesion frequency can be used to probe bond formation without any attempt to measure the relative magnitude of the forces at break-up and by comparing adhesion frequencies for different conditions, the relative adhesive potential of each condition can be assessed (Chesla et al., 1998; Chen et al., 2008).

In this analysis, microcantilevers and micro-beads were both covalently coated with the $(AlaHyp)_{51}$ and/or $(SerHyp_4)_{18}$ glycomodules and any bonds that formed between these glycomodules were detected by applying picoNewton-level forces with the cantilever. We chose the well-characterized $(AlaHyp)_{51}$ and $(SerHyp_4)_{18}$ glycomodules rather than isolated endogenous AGPs or extensins for our assay because they are simple molecules each possessing only one type of glycan thereby making data interpretation straightforward. The intermolecular interactions between these glycomodules were determined in the presence of H^+, Ca^{2+} or boron ions at concentrations that according to the literature mimicked cell wall conditions. This is the first attempt to characterize the interactions between cell wall HRGP glycomodules using an in vitro biophysical approach.

Material and methods

Production of glycomodules

The $(AlaHyp)_{51}$ and $(SerHyp_4)_{18}$ glycomodules were prepared as previously reported (Tan et al., 2003; Shpak et al., 2001). Specifically, synthetic genes encoding $(AlaPro)_{51}$-EGFP and $(SerPro_4)_{18}$-EGFP were expressed in tobacco suspension cultures. The produced fusion glycoproteins were isolated from their culture media, respectively, using a combination of hydrophobic interaction, size-exclusion, and reverse phase chromatographies. The purified $(AlaHyp)_{51}$-EGFP and $(SerHyp_4)_{18}$-EGFP fusion proteins were digested with trypsin to remove the EGFP tags. The released $(AlaHyp)_{51}$ and $(SerHyp_4)_{18}$ glycomodules were re-purified using size-exclusion and reverse phase chromatographies, respectively, as described (Tan et al., 2003; Shpak et al., 2001).

Construction and processing of microcantilevers and micropipettes

Optical fibers of 125 μm diameter (Newport Corp., Irvine, CA) and borosilicate glass tubing of OD 0.9 ± 0.05 mm diameter and wall thickness 0.200 ± 0.013 mm (Friedrich & Dimmock, Millville, NJ) were pulled using a vertical micropipette puller (David Kopf model 730 pipette puller, Tujunga, CA). For fibers, glass was melted using a heater filament and the fibers were extruded by gravity at a rate of 2 mm/s to obtain a long thin cantilever. The extrusion rate was controlled by a hydraulic attachment that used a dashpot containing 75% aqueous glycerol to slow the extension. Cantilevers that were 2–5 μm in diameter at the tip and 10–15 mm long were selected and the cantilever width as a function of axial distance from the tip was measured using optical microscopy. Cantilever stiffness was estimated by fitting an exponential to graphs of cantilever width vs axial distance from the tip and the expected spring constant for an exponentially tapering cantilever was determined from elasticity theory (Landau & Lifschitz, 1986). Calculated cantilever stiffness values ranged from 20–300 pN/μm for the cantilevers were used in the experiments. Since the cantilevers were used only to assess whether a bond had formed or not (which can be done equally well for a range of cantilever stiffnesses), no attempt was made to ensure that all cantilever stiffnesses were exactly the same. Micropipettes were manufactured as described previously (Sundd et al., 2008) using a double pull technique. A custom WPI microforge (Sarasota, FL) system was used to smooth the tips of micropipettes of 4–6 μm inner diameter. The exact micropipette size was determined by insertion of calibrated glass microneedles as described previously (Sundd et al., 2008).

Coating fibers with glycomodules

Pulled fibers were immersed in 20% HCl in 95% ethanol for two hours, then in anhydrous acetone for two hours. The fibers were dipped in a 2% 3-aminopropyltriethoxysilane (3APTS) in acetone solution for 1 min followed by incubation for 24 h at 50 °C in anhydrous acetone containing 2% 3APTS. The fibers were then washed by dipping in the following solutions: acetone for 1 min, dd H_2O for 1 min, acetone for 1 min, dd H_2O for 1 min. The fibers were air dried in a dust-free hood.

The dried fibers were immersed in the wash/coupling buffer (0.1 M MES buffer, pH 7.0) for 10 min, dipped for 2 h in a 10% glutaraldehyde in wash/coupling buffer at room temperature, then washed 3 times with the wash/coupling buffer to remove unreacted glutaraldehyde. The glutaraldehyde derivatized fibers were placed in 1 ml solution of $(AlaHyp)_{51}$ or $(SerHyp_4)_{18}$ glycomodule (dissolved in wash/coupling buffer). The coupling reaction of glycomodules with glutaraldehyde took place through the primary amino groups of either the N-terminus of the proteins or the ε-amino groups of the C-terminus derived from the trypsin digestion (Tan et al., 2003; Shpak et al., 2001). The reaction was incubated at room temperature for 4 h then stopped by dipping in a quenching solution (40 mM glycine in wash/coupling buffer) for 30 min. The fibers were washed 3 times with storage buffer (0.1% NaN_3 in wash/coupling buffer) then stored at 4 °C in storage buffer.

Coupling of glycomodules to the amino beads

Fifty microliter (3.562×10^8 beads/ml) of P(MMA/GlycidylMethAcrylate/EMDA) + NH2 beads (PA06N, Bangs Laboratories, Inc.) were mixed with 5 mg of fresh dry AG 501-X8 resin (20–50 mesh, BIO-RAD) for 1 h at room temperature. The beads were derivatized with glutaraldehyde and $(AlaHyp)_{51}$ glycomodule, $(SerHyp_4)_{18}$ glycomodule, or BSA as described above for fiber derivatization, except the beads were harvested by centrifugation for 3 min at 3000g after each step.

Amino acid composition analysis and determination of coating efficiency

To quantify the glycomodules on fibers or beads, coated fibers or beads were hydrolyzed with 6 N HCl at 110 °C (gas phase) under vacuum for 20 h. The particulate was removed from the hydrolysis by centrifugation, followed by four washes of the particulate with 6 N HCl. The HCl solution and washes were combined and the HCl removed by evaporation under a flow of N_2 gas. The hydrolysate was derivatized with phenyl isothiocyanate (PITC) at room temperature for 20 min, the reaction terminated by degassing under vacuum (Bergman et al., 1986). The derivatized amino acids were separated on a Prodigy ODS column (Phenomenex, 150 × 4.60 mm, 3 µm), equilibrated with Buffer A (0.03 M sodium hydroxide titrated to pH 6.60 with 1 M o-phosphoric acid) and gradient-eluted at 1 ml/min. The effluent was monitored at 254 nm. The gradient was: 0–1 min 0–5% Buffer B; 1–27 min 5–37% Buffer B (Buffer B: 60% acetonitrile in water).

To determine the coating efficiencies (number of molecules/1000 nm^2 of surface), beads and fibers (un-pulled) were coated with $(AlaHyp)_{51}$ glycomodule using solutions of different glycomodule concentrations (0, 2.02, 4.38, 8.40, 9.65, and 12.90 mg/ml for fibers; 0, 1.69, 3.65, 7.00, 8.04, 10.75 mg/ml for beads) or $(SerHyp_4)_{18}$ glycomodule solutions of concentrations (0, 0.64, 1.08, 1.29, 2.18, and 4.38 mg/ml for fibers; 0, 0.61, 1.03, 2.08, 4.17 mg/ml for beads). The amount of bound $(AlaHyp)_{51}$ or $(SerHyp_4)_{18}$ glycomodule was determined by amino acid composition analysis, using $(AlaHyp)_{51}$ or $(SerHyp_4)_{18}$ glycomodules as standards and norleucine as an internal standard. The coating efficiencies were determined based on the numbers of bound glycomodules (= amount of bound glycomodule in mol × 6.022×10^{23} mol^{-1}) and the calculated surface area (fiber area = πDL; D: diameter of the fiber (125 µm), L: length of fiber (38 cm); bead area = $4\pi r^2$, r: bead average radius (7.74/2 µm)).

Microcantilever setup

Viewing chamber

Coated microcantilevers were mounted in a specially constructed viewing chamber (Fig. 1A). The lexan chamber was composed of notched top half and bottom half chambers, with the notches allowing insertion of fibers (Tees et al., 2001). The two halves of the chamber were assembled and sealed with silicone sealant. One wall of the chamber was left open, to allow for insertion of micropipettes. The chamber was filled and flushed from a flow inlet (Tees et al., 2001).

Micromanipulation

The viewing chamber was placed on the stage of an inverted microscope (Fig. 1B). Coated bead suspensions were introduced into the viewing chamber and individual beads were selected and aspirated onto the tips of micropipettes using a custom built manometer (Tees et al., 2001) (Fig. 1B). Aspiration pressure was recorded by pressure transducer (Model CD223, Validyne Corp., Northridge, CA). The micropipette was mounted in series with a computer-controlled piezoelectric actuator (Melles Griot, Boulder, CO) that applied a precisely controlled retraction velocity to the micropipette and bead. For initial positioning and manipulation of the bead, the actuator and micropipette were mounted on a hydraulic micromanipulator (Narishige, Fryer Corp, Huntley, IL). This was mounted, in turn, on a coarse manipulation system (Newport Corp., Irvine, CA), to allow control over five translational and rotational degrees of freedom. The entire assembly was mounted on a vibration isolation table (Newport Corp, Irvine, CA). The bead and fiber were viewed through the microscope with a CCD video camera, displayed on a video monitor, and recorded on videocassette for later image analysis.

Forced unbinding experiments

Forced unbinding experiments were performed using the microcantilever system described above. The viewing chamber was filled with TBS ranging from pH 5.5 to pH 9.5. Micropipettes attached to the micro/nanomanipulation system were introduced through the open end of the viewing chamber. A glycomodule-coated bead was aspirated onto the micropipette tip. An apposition test cycle for forced unbinding consisted of the following four steps (the first three steps are shown in Fig. 2):

1) *apposition* (Fig. 2A): a bead was held in contact with a microcantilever for one second. The cantilever was given a small initial negative deflection (representing a contact force of < 100 pN) to ensure that bead and cantilever were in contact.
2) *retraction* (Fig. 2B): the bead was retracted at a velocity of ~25 µm/s. If a bond exists between bead and cantilever, then the cantilever deflected past its rest position leading a detectable adhesive event.
3) *hold* (Fig. 2C): the fully retracted bead position was held for one second to allow the cantilever to relax to its rest position.
4) *return*: the bead was returned to its initial position to start the next cycle.

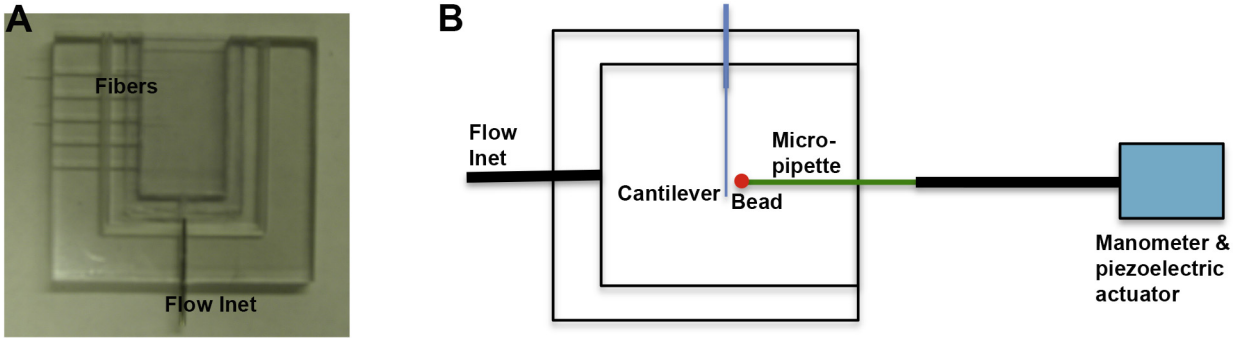

Fig. 1. Instrumental setup of microcantilever and microscope. (A) Viewing chamber. Two half chambers were sealed to mount the tips of microcantilevers in the chamber. The upper wall was open to allow insertion of micropipettes. The bottom flow inlet was used to change buffers or wash microcantilevers. (B) The chamber was mounted on the stage of a microscope and the micropipette was mounted in series with a computer-controlled piezoelectric actuator that applied a range of precisely controlled retraction velocities to the pipette and bead. A custom built manometer was used to aspirate bead onto the tip of a micropipette.

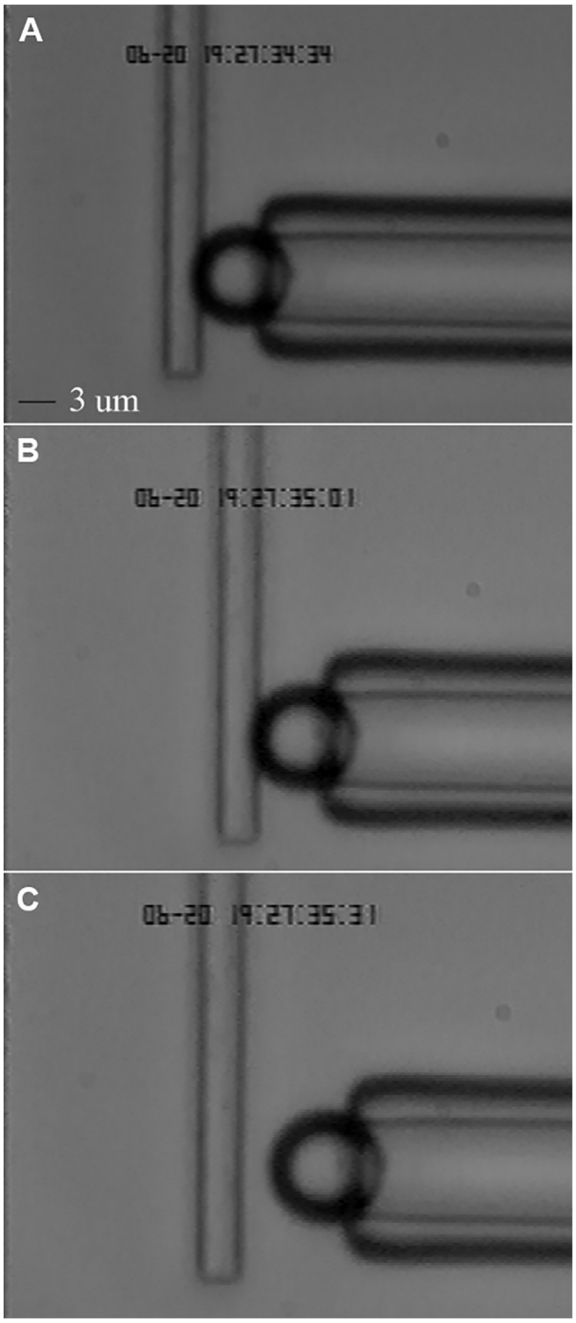

Fig. 2. Images of a forced unbinding experiment. (A) The image shows the stage of apposition. A bead was held in contact with a microcantilever. The cantilever was given a small initial negative deflection to ensure that bead and microcantilever were in contact. (B) The image shows the retraction stage. The bead was retracted at a velocity of ~25 μm/s to the right side in the image. (C) The image shows the hold stage, in which the microcantilever is allowed to relax to its rest position. After the hold stage, the bead returned to the apposition position and another test cycle begins.

Hundreds of test cycles were recorded for analysis. Video images of the events were captured to a PC and analyzed frame-by-frame with Labview and IMAQ Vision (National Instruments, Austin, TX). The centroid of the cantilever (and the bead) were determined to within ~10 nm resolution. Distances on the video were calibrated using a stage micrometer (Fisher Scientific, Hanover Park, IL). Adhesive events were defined by durable microcantilever deflection, as shown at 18 s in Fig. 3. A representative video showing one adhesion event in five test cycles was also presented as Supplemental Video 1. The percentage of

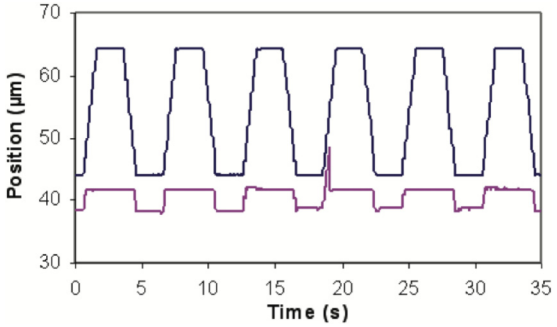

Fig. 3. Graph of bead and microcantilever positions as a function of time. The positions of the bead (upper blue line) and microcantilever (lower purple line) above were monitored and analyzed, which gave the graph. The long flat stages of the purple line showed the resting positions of cantilever, while the short flat stages of the purple line showed the positions that cantilever contacted with the bead. One adhesive event occurred at the 18 s mark. (For interpretation of the references to colour in this figure legend, the reader is referred to the web version of this article.)

all apposition tests that resulted in unbinding events was calculated for each test condition.

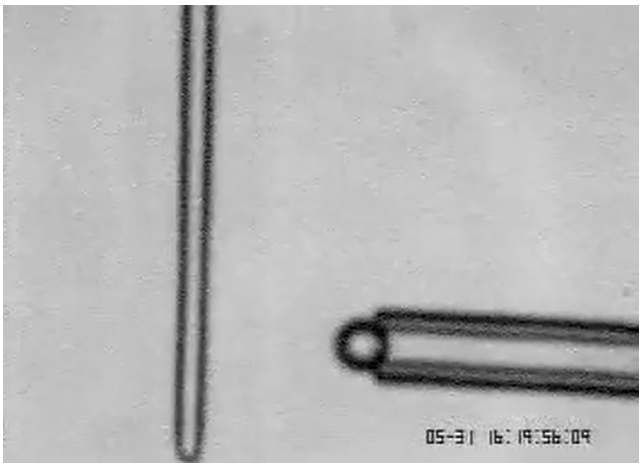

Video 1.

Conditions used for adhesion tests

Bead-glycomodule to microcantilever-glycomodule adhesion tests were carried out in the following buffers: 20 mM Tris-buffered saline (TBS) buffer in 50 mM EDTA at pH 5.5, 7.5, and 9.5; 20 mM Tris-buffered saline (TBS) buffer in 0.5 mM $CaCl_2$ (Hepler, 2005) at pH 5.5; 20 mM Tris-buffered saline (TBS) buffer in 10 mM boric acid (Matoh, 1997) and 50 mM EDTA at pH 5.5.

Error analysis and statistics

Adhesive event frequencies are determined by the ratio of events to the total number of tests. The number of events should follow the binomial distribution. Standard formulas are available for the upper and lower 95% confidence interval of the adhesive event frequencies (Sachs, 1984) and these are shown as error bars in Figs. 5A, 6A, and 6B. The p values associated with differences between adhesion frequencies were determined using the relations in Sections 4.5 and 4.6 of Sachs (1984). Bonferroni correction was used to compensate for multiple comparisons, but even with that compensation, all frequency differences noted in the Results and Discussion were highly significant with $p \ll 0.001$.

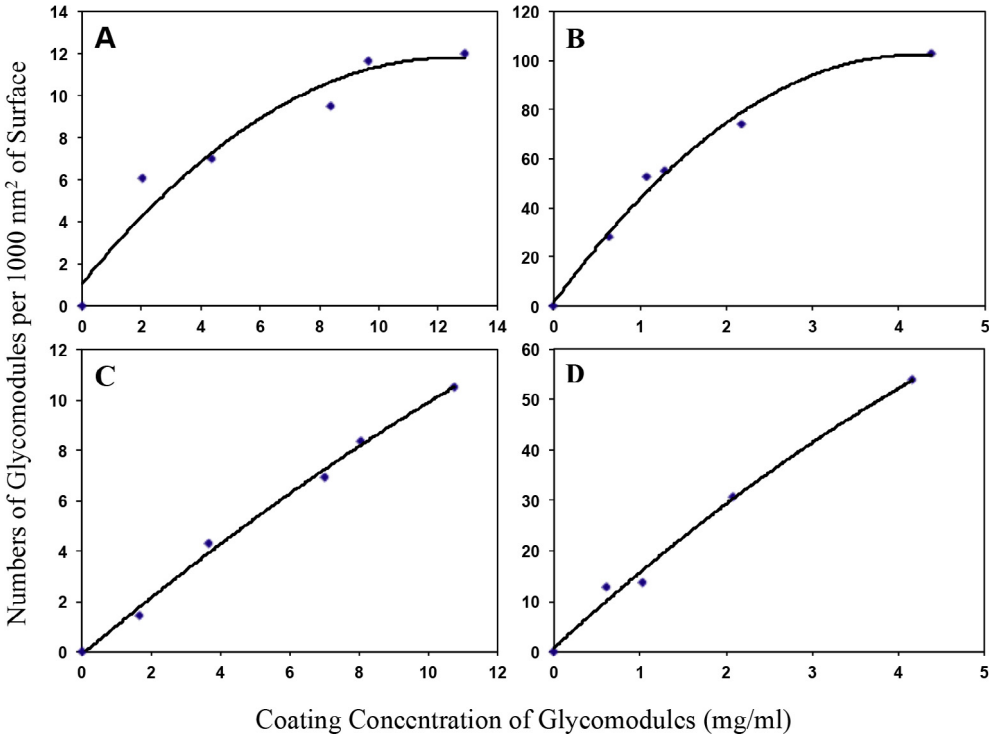

Fig. 4. Correlation between coating concentration of $(AlaHyp)_{51}$ or $(SerHyp_4)_{18}$ glycomodules and numbers of coated glycomodules on 1000 nm^2 surface on microcantilever or beads. $(AlaHyp)_{51}$ or $(SerHyp_4)_{18}$ glycomodules were used to coat at a ranging of concentrations. The total amount of the glycomodule was determined by amino acid composition analysis. The numbers of the glycomodule on 1000 nm^2 area on either fibers or beads were calculated from the surface of the used fibers or beads. (A) $(AlaHyp)_{51}$ glycomodules on fibers; (B) $(SerHyp_4)_{18}$ glycomodules on fibers; (C) $(AlaHyp)_{51}$ glycomodules on beads (one mg of beads has 3.432×10^6 particles, the mean diameter of beads is 7.74 μm.); and D. $(SerHyp_4)_{18}$ glycomodules on beads.

Results and discussion

Coupling $(AlaHyp)_{51}$ or $(SerHyp_4)_{18}$ glycomodules to the fibers or beads

Beads or fibers prior to pulling were coupled with each glycomodule at a range of concentrations. Amino acid composition analyses quantified the amounts of glycomodules on the coated fibers or beads. The surface area of the derivatized fibers or beads was calculated from their lengths and/or diameters. Given the estimated molecular mass of 132 kDa for $(AlaHyp)_{51}$ glycomodule and 66.4 kDa for $(SerHyp_4)_{18}$ glycomodule (Tan et al., 2004; Shpak et al., 2001), we correlated the coating concentrations of the glycomodules to the numbers of molecules per 1000 nm^2 surface on the coated fibers or beads as shown in Fig. 4.

Microcantilevers that were coated with glycomodule at concentrations below 2 mg/ml showed no measurable adhesion to coated beads. Thus for the microcantilevers, we chose coating concentrations for the $(AlaHyp)_{51}$ glycomodule of 3 mg/ml and 2 mg/ml for the $(SerHyp_4)_{18}$ glycomodule, both concentrations were less than their saturation concentrations (Fig. 4A and B). Based on the relationship curves shown in Fig. 4A and B, the selected coating concentrations were estimated to be 6 $(AlaHyp)_{51}$ or 70 $(SerHyp_4)_{18}$ glycomodules per 1000 nm^2 surface on the fibers. Beads were coupled with glycomodules at two or more diluted concentrations for selection of beads with different numbers of glycomodules/1000 nm^2 surface for forced unbinding tests.

The adhesion of AGP and extensin glycomodules is specific and pH dependent

To determine if the interactions measured were specific or simply a general nonspecific adhesion phenomenon, we measured the adhesion between the glycomodules and BSA (66 kDa) at pH 7.5. In this experiment, the beads were coated with approximately 70 BSA molecules per 1000 nm^2. Our results showed that the control protein BSA did not adhere to either of these two glycomodules, with the frequency of adhesive events at 0.3% between BSA and the $(AlaHyp)_{51}$ glycomodules and at 1.3% between BSA and the $(SerHyp_4)_{18}$ glycomodules. Using the same cantilevers and test buffer, when we switched to beads bearing 2 $(AlaHyp)_{51}$ per 1000 nm^2 surface, we recorded a 12.5% adhesive event rate between the $(AlaHyp)_{51}$ glycomodules on bead and microcantilever (Fig. 5A). Similarly, when we switched to beads with 30 $(SerHyp_4)_{18}$ glycomodules per 1000 nm^2 surface, we recorded a 23.1% adhesive event rate between the $(SerHyp_4)_{18}$ glycomodules on bead and microcantilever. In addition, no significant adhesion was measured between the $(AlaHyp)_{51}$ and $(SerHyp_4)_{18}$ glycomodules under these conditions. These data suggest that the intermolecular adhesion is specific.

To monitor the effect of H^+ on adhesion between these glycomodules, we varied the pH of the test buffer. With the same set up as above, the intermolecular adhesive event rate between the $(AlaHyp)_{51}$ glycomodule decreased significantly from 12.5% to 0% as pH increased from 7.5 to 9.5. However, when the pH dropped to 5.5, the bond formed was too strong to be broken in the test cycles. We switched to beads coated with one $(AlaHyp)_{51}$ glycomodule per 2000 nm^2 surface (coated at 0.5 mg/ml) to reduce the numbers of interacting molecules (Fig. 4C). The intermolecular adhesive event rate between the $(AlaHyp)_{51}$ glycomodules was 58.3% over many test cycles (Fig. 5A).

Acidic pH favored the interactions between AGP glycomodules, most likely due to the presence of 15 mole percent of GlcA in the $(AlaHyp)_{51}$ glycomodule (Tan et al., 2003). At pH 5.5, although the carboxyl groups of GlcA residues were completely deprotonated, the carbonyl oxygen of the ionized GlcA could H-bond with neighboring molecules via interacting with a proton on a nearby hydroxyl. The interaction of H^+ with the hydroxyl oxygen enhanced the H-bonding between the hydroxyl proton and the carbonyl oxygen (Fig. 5B). The formed intermolecular H-bonds resulted in a significant increase of adhesion between $(AlaHyp)_{51}$ glycomodules at this pH. On the other hand, when the pH was increased to 9.5, protons were being pulled off the sugar hydroxyls, resulting in negative charges on sugar residues. In this situation, charge repulsion should prevent any intermolecular interactions (Fig. 5B), leading to no detectable adhesion between the $(AlaHyp)_{51}$ glycomodules.

In contrast, the adhesion between $(SerHyp_4)_{18}$ glycomodules displayed a different pH-dependent pattern. The $(SerHyp_4)_{18}$ glycomodules showed no intermolecular adhesion at pH 9.5, but the adhesion events decreased from 23.1% to 8.3% when the pH dropped from 7.5 to

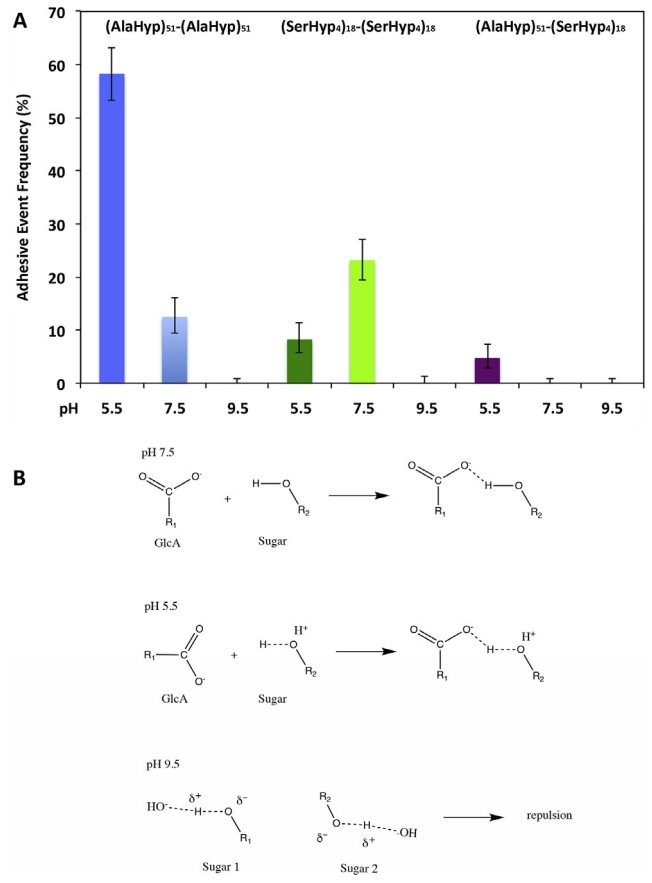

Fig. 5. Adhesion events recorded during the homomolecular and heteromolecular interactions of the glycomodules at different pH condition (A) and the possible adhesion mechanisms (B). (A) The microcantilevers were coated with 6 $(AlaHyp)_{51}$ glycomodules per 1000 nm^2 or 70 $(SerHyp_4)_{18}$ glycomodules per 1000 nm^2. The beads used for $(AlaHyp)_{51}$ to $(AlaHyp)_{51}$ glycomodule adhesion at pH 9.5 and 7.5 were coated with 2 $(AlaHyp)_{51}$ glycomodules/1000 nm^2, while with 1 $(AlaHyp)_{51}$ glycomodule/2000 nm^2 for $(AlaHyp)_{51}$ homomolecular adhesion at pH 5.5. The $(SerHyp_4)_{18}$ glycomodule beads were coated with 30 molecules/1000 nm^2. The adhesive event rate was measured as a percentage of adhesive events from hundreds of test cycles. (B) At pH 7.5, H-bonds are formed between GlcA and hydroxyls of other sugars; while at pH 5.5 hydroxyl proton that is loosely attached to hydroxyl oxygen due to the attack of H^+ on the hydroxyl oxygen forms stronger H-bond with oxygen of GlcA carbonyl. However, at pH 9.5, the hydroxyl proton is pulled off by ^-OH, which resulted in a partially negatively charged sugar. The negative charges of different sugars repel each other and prevent intermolecular adhesion.

5.5 (Fig. 5A). Since $(SerHyp_4)_{18}$ glycomodules contain only neutral sugars (Gal 5% and Ara 95% in mole percent), H-bonds would form mainly between the hydroxyl groups. At pH 5.5, H^+ would interact with oxygen atoms of hydroxyls, which likely weakens intermolecular H-bonding between hydroxyls of neutral sugar residues. At pH 9.5, like $(AlaHyp)_{51}$, protons were being pulled off the hydroxyls of arabinosyl residues, and charge repulsion would dominate the intermolecular interaction that resulted in no adhesion. Thus, the $(SerHyp_4)_{18}$ glycomodules only showed moderate adhesion at neutral pH. In addition, the carbonyl groups from the peptide amide bonds can also form H-bonds with the hydroxyls, however, in the instance of Hyp in the $(AlaHyp)_{51}$ glycomodule, each Hyp is glycosylated with an arabinogalactan polysaccharide and each Hyp or Ser of the $(SerHyp_4)_{18}$ glycomodule is glycosylated with an arabinooligosaccharide or a single Gal residue, respectively. Thus the amides might be shielded by the sugars, which is consistent with our results.

Furthermore, no adhesion was observed between $(AlaHyp)_{51}$ glycomodules (6 glycomodules per 1000 nm^2 on microcantilever) and $(SerHyp_4)_{18}$ glycomodules (30 glycomodules per 1000 nm^2 on beads) when the pH increased to 9.5, but weak adhesion with a 4.8% adhesion event was recorded when the pH decreased to pH 5.5 (Fig. 5). This pattern is attributed to the same mechanism described for the interaction between $(AlaHyp)_{51}$ glycomodules, while less heteromolecular adhesion may result from the lack of carboxyl groups (or GlcA residues) and fewer hydroxyls/sugar residues being present in the $(SerHyp_4)_{18}$ glycomodules.

It is believed that the pH of plant cell walls, especially the cell walls of growing cells, is around 5.5 (Cosgrove, 2005). For example, the cell walls of root hair initiation sites have a localized pH ranging from 5.0 to 4.5, while the pH of the rest cell walls is 6.0 (Bibikova et al., 1997). To mimic the wall pH condition, we chose pH 5.5 for the subsequent adhesion measurements.

The adhesion of AGP and extensin glycomodules is Ca^{2+} dependent at pH 5.5

In our in vitro measurement, when Ca^{2+} ions were added to the test buffer to a final concentration of 0.5 mM (pH 5.5, in 20 mM TBS) (Hepler, 2005), and microcantilevers were coated with six $(AlaHyp)_{51}$ glycomodules per 1000 nm^2 and beads coated with one $(AlaHyp)_{51}$ glycomodule per 2000 nm^2, the adhesive event rate between $(AlaHyp)_{51}$ glycomodules increased dramatically from 58.3% to 84.5% (Fig. 6A). Similarly, the intermolecular adhesion events between $(SerHyp_4)_{18}$ glycomodules increased from 8.3% to 30%, when there was about 70 $(SerHyp_4)_{18}$ glycomodules per 1000 nm^2 of microcantilever and ~30 $(SerHyp_4)_{18}$ glycomodules per 1000 nm^2 of bead (Fig. 6A). In addition, the heteromolecular adhesive event rate also increased significantly from 4.8% to 45.7% in the presence of Ca^{2+} (Fig. 6A), when the microcantilevers had six $(AlaHyp)_{51}$ glycomodules per 1000 nm^2 and the beads about 30 $(SerHyp_4)_{18}$ glycomodules per 1000 nm^2. These results suggest that Ca^{2+} ions can enhance both the homomolecular and heteromolecular adhesion between these glycomodules, and indicate that the interaction between those glycomodules is Ca^{2+} dependent.

Ca^{2+} ions are an important component of plant cell wall. In addition to serving as signaling molecules, divalent calcium ions have a radius suitable for forming strong complexes via calcium bridges with 6-membered ring glycans having a contiguous *a,e,a* sequence of hydroxyls or 5-membered ring carbohydrates possessing cis,cis-1,2,3 triol groups (Angyal, 1989). Some sugar residues can also form complexes with calcium by adopting conformational changes to have those *a,e,a* or cis,cis-1,2,3 triol groups or tri-oxygens at appropriate distances. Furthermore, Ca^{2+} ions can form strong bonds with wall glycopolymers containing carboxyl groups such as pectins and AGPs (Caffall and Mohnen 2009; Lamport and Varnai, 2013). It was estimated the molar ratio of GlcA:Ca^{2+} in most AGPs is about 2 to 3.8 (Lamport and Varnai, 2013). The strong Ca^{2+} bridge formed with carboxyl groups of GlcA would explain the significant increase of adhesion between the $(AlaHyp)_{51}$ glycomodules in the presence of Ca^{2+} (Tajmir-Riahi, 1983).

Although $(SerHyp_4)_{18}$ glycomodules do not contain GlcA residues, we still recorded a significant increase of adhesion between the extensin glycomodules after addition of Ca^{2+}. The hydroxyls of t-Gal and/or t-Ara residues on $(SerHyp_4)_{18}$ glycomodules may undergo conformational changes to possess triol groups or tri-oxygen atoms that favor Ca^{2+} bridge formation. The same mechanisms may be applied to the heteromolecular interaction between the AGP and extensin glycomodules. The carboxyl groups from the AGP glycomodules and the conformationally changed triol groups/tri-oxygen atoms from the extensin glycomodules might form calcium bridges with Ca^{2+}, resulting in dramatic increases of the adhesion between these two glycomodules. However, because of the energy barrier for sugar conformational changes and lack of carboxyls, the adhesive event rates in these two cases were much less than that between the AGP glycomodules.

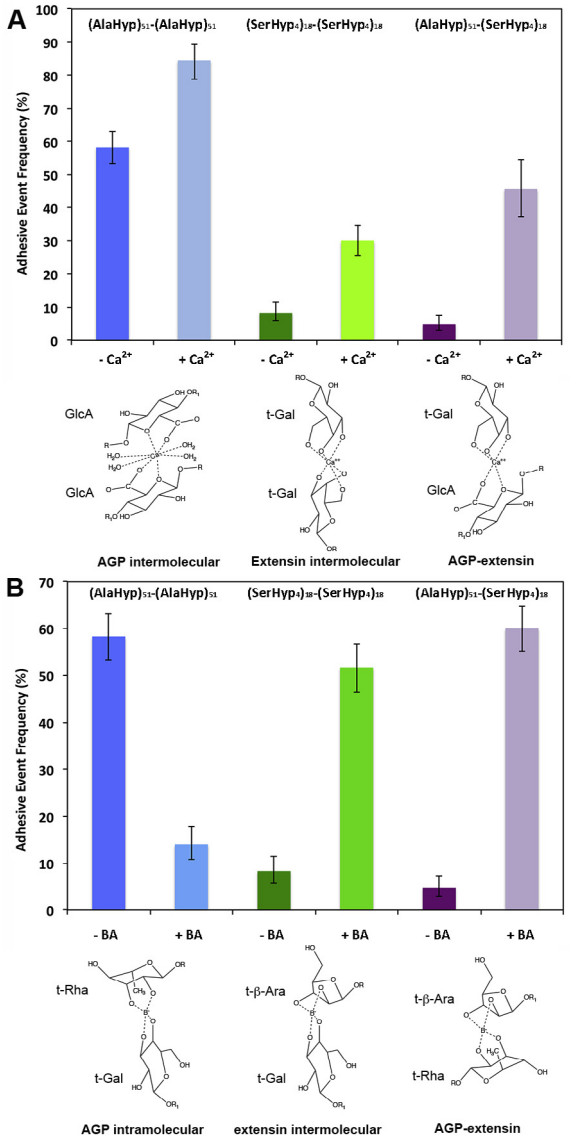

Fig. 6. Adhesive event rates recorded during the homomolecular and heteromolucular interactions of the glycomodules in the presence of Ca^{2+} (A) or boron (B) at pH 5.5 and the possible adhesion mechanisms. The microcantilevers were coated with 6 $(AlaHyp)_{51}$ glycomodules/1000 nm^2 or 70 $(SerHyp_4)_{18}$ glycomodules/1000 nm^2. The beads used for $(AlaHyp)_{51}$ to $(AlaHyp)_{51}$ glycomodule adhesion were coated with 1 $(AlaHyp)_{51}$ glycomodule/2000 nm^2, while the $(SerHyp_4)_{18}$ glycomodule beads were coated with 30 molecules/1000 nm^2. The final concentration for Ca^{2+} was 0.5 mM and for boric acid (BA) was 10 mM. For the possible adhesion mechanisms, representative sugars were selected for presenting the predicted calcium bridges or borate esters between or within the glycomodules.

The adhesion of AGP and extensin glycomodules is boron dependent at pH 5.5

Boron is required by all living organisms having carbohydrate-rich cell walls or cell envelopes (Loomis and Durst, 1991). The chemical base is the spontaneously formation of tetrahedral cyclic borate diester cross-links with cis-dihydroxyls in pectic polysaccharides, glycoproteins, glycolipids, and o-diphenolics (Bolanos et al., 2004). The most stable borate diesters are those reacted with cis-diol containing furanoses such as ribose and apiose, since they have optimal distances between two hydroxyls and corresponding low steric hindrance (Henderson et al., 1973; Loomis and Durst, 1992). Cis-diol containing pyranoses would take a specific conformation to make the cis-diol close enough to form the diester bonds and the relatively unstable borate pyranose diester complexes. The function of borate in cell walls is exemplified by its capacity to form borate diesters with apiosyl residues on rhamnogalacturonan II (RG-II) sides chains and hence cross-link RG-II molecules in vivo (O'Neill et al., 2001).

In order to monitor the possible effect of boron on AGP and extensin glycomodules, we added boric acid to the test buffer to a final concentration of 10 mM (final pH 5.5) (Matoh, 1997; Power and Woods, 1997). With all other conditions the same as those used to test Ca^{2+} ion effects, we noted that the homomolecular adhesion events between $(AlaHyp)_{51}$ glycomodules decreased significantly from 58.3% to 14%, while the homomolecular adhesion events between $(SerHyp_4)_{18}$ glycomodules increased significantly from 8.3% to 51.6% (Fig. 6B). Interestingly, the heteromolecular adhesion event between $(AlaHyp)_{51}$ and $(SerHyp_4)_{18}$ glycomodules also increased dramatically from 4.8% to 60% (Fig. 6B).

These results indicate that the conformations of some sugar residues were altered to favor the formation of borate diester bonds, both intramolecularly and intermolecularly. Although the major sugar residues in $(AlaHyp)_{51}$ glycomodules such as 3-Gal*p*, 3,6-Gal*p*, t-GlcA*p*, 4-GlcA*p*, and α-Ara*f* do not have cis-diols, 3,4-diols in t-Gal*p* and 6-Gal*p* and 2,3-diols in t-α-Rha*p* residues might adopt a twisted boat or chair conformation to form relatively stable borate ester bonds. This would allow intramolecular cross-linking of these peripheral sugar residues with borate and subsequently block the formation of intermolecular H-bonding between GlcA carboxyl groups and hydroxyl groups, and consequently decrease adhesion between these AGP glycomodules.

Similarly, the 5% t-Gal residues of the $(SerHyp_4)_{18}$ glycomodule possess cis-diols, which might contribute to the borate diester formation between the extensin glycomodules. However, the dramatic increase of adhesion between the extensin glycomodules introduced by borate indicates that the majority Ara*f* residues may also participate in forming borate diesters. Since $Hyp\text{-}Ara_4$ and $Hyp\text{-}Ara_3$ have linkages such as α-L-Ara*f*-(1–3)-β-L-Ara*f*-(1–2)-β-L-Ara*f*-(1–2)-β-L-ara*f*-(1–4)-Hyp and β-L-Ara*f*-(1–2)-β-L-Ara*f*-(1–2)-β-L-ara*f*-(1–4)- Hyp, only terminal Ara*f* residues in the $(SerHyp_4)_{18}$ glycomodules contain contiguous diol groups. In addition, excepting the terminal α-Ara*f* residues in $Hyp\text{-}Ara_4$, all other terminal Ara*f* residues in $Hyp\text{-}Ara_3$, $Hyp\text{-}Ara_2$, and Hyp-Ara are β-linked. The anomeric β-configuration may force the cis hydroxyl on the 2-position (2-OH) to orient far from the glycosidic bond but close to 3-OH, which favors the formation of borate diester bond between two t-β-Ara*f* residues. Furthermore, the different lengths and molar populations of the Hyp-arabinosides, including 32% Hyp with Ara_4, 56% Hyp with Ara_3, 9% Hyp with Ara_2, and 3% Hyp with Ara_1, as well as the locations of these arabinosides along the polypeptide, make the extent of intramolecular borate diester bond formation unfavorable. The observed greater adhesion between the extensin glycomodules suggests that the t-β-Ara*f* residues and t-Gal*p* contributed to the formation of intermolecular borate diester bonds. Considering the reasons listed above, the significantly increased heteromolecular adhesion might be due to the formation of relatively stable borate diester bonds between the t-Rha*p* or t-Gal*p* residues on $(AlaHyp)_{51}$ glycomodules and the t-β-Ara*f* or t-Gal*p* residues on $(SerHyp_4)_{18}$ glycomodules.

Possible functions of AGPs and extensins through interactions regulated by wall ions

Among the cell wall-bound ions, protons, calcium and boron are essential for plant growth. Calcium and boron are mainly immobile in mature tissues of plants, as both calcium and boron cannot be released from cell walls by extensive water or dilute alkali washes. However, dilute HCl can extract most of boron and calcium from cell walls at room temperature. This suggests both boron and calcium form pH-dependent complexes in cell walls (Brown and Hu, 1994). Proton is deemed to be a major wall-loosening factor. It is believed that low pH can activate the cell wall enzymes/proteins such as expansins and

subsequently break non-covalent bonds between cellulose and other wall polysaccharides (Cosgrove, 2005). This results in loosening of the cell walls and allows elongation or expansion of cells.

The question then arises: what would compensate the broken non-covalent bonds in the loosened walls? For example, pollen elongation requires wall loosening in the elongation zone. Immunohistolocalization showed that pollen tube walls are mainly composed of callose, cellulose, pectins and AGPs (Taylor and Hepler, 1997). We hypothesize AGPs play an important role in these biological processes because among those wall polymers only AGPs are anchored to the plasma membrane through C-terminal GPI anchors. Although we do not know the exact numbers of AGPs bound on pollen tube plasma membrane, the plasma membrane of a single tobacco BY-2 cell was estimated having $1x10^{15}$ bound AGP molecules (Lamport and Varnai, 2013). In our experiments, the contact area of a bead and a microcantilever was about 0.25 μm^2 (± 4%). On such a contact area, about 125 $(AlaHyp)_{51}$ glycomodules on the bead and 1500 $(AlaHyp)_{51}$ glycomodules on the microcantilever contributed to the intermolecular adhesion. Furthermore, at the unbinding point, the unbinding force was in the range of 20–100 pN. The generated pressure on the contact surface would be around 800–4000 bar, comparing to the reported hydrostatic pressure of a growing root cell at about 6 bars (Fricke et al., 2000). Therefore in the presence of wall H^+ and Ca^{2+}, the adhesion between neighboring AGPs anchored on the outside of plasma membrane may provide enough attractive forces during wall elongation or expansion to tighten the plasma membrane against the inside turgor pressure.

In another biological process, AGPs were found to display an increasing gradient of glycosylation along the transmitting tissue from the stigma end to the ovary end, consistent with the pollen tube elongation direction (Cheung et al., 1996). Coincidently, an increasing gradient of Ca^{2+} in style from stigma end to ovary end was found in *Antirrhinum majus* (Mascaenhas and Machlis, 1962). A high level of Ca^{2+} was also identified in the cell wall of embryo sac after pollination (Zhao et al., 2002). These two gradients lead us to speculate that molecules such as AGPs on pollen tube tip may interact with AGPs along the transmitting tissue, and the gradually increased interaction force may direct the elongation of pollen tube. This hypothesis is supported by the observation that antisense-suppressed transgenic plants of TTS (transmitting tissue-specific) protein, an AGP, showed a reduced pollen growth rate (Cheung, 1996). Thus, calcium may be a critical factor to some plant functions through manipulating AGP adhesion.

Boron is continually required throughout the life of vascular plants and diatoms. Matoh et al. (1992) found that more than 95% of cell boron is present in the cell walls of cultured tobacco BY2 cells. Boron deficiency causes slowing and cessation of root elongation and cell wall fragility, while boron excess makes plants produce unusually resilient cell walls. For example plant growth ceases in culture medium with a boron concentration beyond 30 mM (Loomis and Durst, 1992). Most boron in cell walls is believed to complex with pectic polysaccharides through the borate-apiose diester bonds. Borate diester bonds are sensitive to pH. It is believed that the bonds are broken when cell wall pH is lower than 4.4 occurred in pH drop during auxin-activated acid growth that allows RG-II to slide past each other (Hu and Brown, 1994; Matoh, 1997). While the pH of cell walls increases, the borate bonds form again. This mechanism makes the cell wall expansion possible. However, ^{11}B NMR analysis showed that only 80% of borate complexes were with RG-II (Kobayashi et al., 1997), indicating that about 20% of cell wall boron is bound to other wall components. Our results suggest that some of the boron may form relatively unstable diester bonds intermolecularly or intramolecularly with extensins and/or AGPs and indicates that the borate-regulated interactions between extensins and/or between extensins and AGPs may function in plant cell walls, especially in monocot walls that are pectin-poor.

We used a simplified condition in this experiment, with which only HRGP glycomodules were analyzed and the effects of cellulose, hemicellulose, and pectin were not considered. This may be similar in vivo for classic AGPs that are anchored on plant cell plasma membrane facing the apoplast via GPI-anchors. The cell surface AGPs may interact similarly to our experimental design. This setup for forced unbinding experiment may be used to further analyze adhesions between AGPs/extensins and other wall components, such as pectins and soluble hemicelluloses, or between other wall components. Although this method only measures the adhesion between two wall components at a time, it will generate more interaction patterns between different wall polymers, and help us understand the contribution of intermolecular adhesion/interaction to wall integrity and architecture from the view of biophysics.

Conclusion

In conclusion, AGP and extensin glycomodules show different homomolecular and heteromolecular adhesion patterns in the presence of different wall ions such as H^+, Ca^{2+}, and borate. Adhesion changes regulated by different wall ions may modulate the interactions of AGPs and/or extensins in specific biological process. Although the in muro situation is more complicated perhaps involving AGP-extensin hybrids and complexes of AGPs with other wall polysaccharides such as pectin, our in vitro analysis would provide insights at molecular level for understanding possible functions of AGPs and extensins in vivo.

Declarations of interest

None.

Acknowledgement

This work was supported by the Herman Frasch Foundation – United States [grant number 526-HFJ02].

Author contribution

LT, DT, and MJK designed the experiments. LT wrote the manuscript. LT, DT, and MJK revised the manuscript. LT, SK, and JQ performed the experiments. All authors participated in data analysis.

References

Akiyama, Y., Mori, M., Kato, K., 1980. ^{13}C-NMR analysis of hydroxyl-proline arabinosides from *Nicotiana tabacum*. Agric. Biol. Chem. 44, 2487–2489. http://dx.doi.org/10.1080/00021369.1980.10864347.

Angyal, S.J., 1989. Complexes of metal cations with carbohydrates in solution. Adv. Carbohydr. Chem. Biochem. 47, 1–43. http://dx.doi.org/10.1016/S0065-2318(08)60411-4.

Arya, M., Kolomeisky, A.B., Romo, G.M., Cruz, M.A., López, J.A., Anvari, B., 2005. Dynamic force spectroscopy of glycoprotein Ib-IX and von Willebrand Factor. Biophys. J. 88, 4391–4401. http://dx.doi.org/10.1529/biophysj.104.046318.

Bergman, T., Carlquist, M., Jornvall, H., 1986. Amino acid analysis by high performance liquid chromatography of phenylthiocarbamyl derivatives. In: Wittmann-Liebold, B., Salnikow, J., Erdmann, V.A. (Eds.), Advanced Methods in Protein Microsequence Analysis. Springer, Berlin, Heidelberg, pp. 45–55 https://doi.org/10.1007/978-3-642-71534-1_5.

Bibikova, T.N., Zhigilei, A., Gilroy, S., 1997. Root hair growth in Arabidopsis thaliana is directed by calcium and an endogenous polarity. Planta 203, 495–505. http://dx.doi.org/10.1007/s004250050219.

Bolanos, L., Lukaszewski, K., Bonilla, I., Blevins, D., 2004. Why boron? Plant Physiol. Biochem. 42, 907–912. http://dx.doi.org/10.1016/j.plaphy.2004.11.002.

Brown, P.H., Hu, H., 1994. Boron uptake by sunflower, squash and cultured tobacco cells. Physiol. Plant. 91, 435–441. http://dx.doi.org/10.1111/j.1399-3054.1994.tb02971.x.

Caffall, K.H., Mohnen, D., 2009. The structure, function, and biosynthesis of plant cell wall pectic polysaccharides. Carbohydr. Res. 344, 1879–1900. http://dx.doi.org/10.1016/j.carres.2009.05.021.

Cannon, M.C., Terneus, K., Hall, Q., Tan, L., Wang, Y., Wegenhart, B.L., Chen, L., Lamport, D.T.A., Chen, Y., Kieliszewski, M.J., 2008. Self-assembly of the plant cell wall requires an extensin scaffold. PNAS 105, 2226–2231. http://dx.doi.org/10.1073/pnas.0711980105.

Chen, W., Evans, E.A., McEver, R.P., Zhu, C., 2008. Monitoring receptor-ligand interactions between surfaces by thermal fluctuations. Biophys. J. 94, 694–701. http://dx.

doi.org/10.1529/biophysj.107.117895.
Chen, Y., Dong, W., Tan, L., Held, M.A., Kieliszewski, M.J., 2015. Arabinosylation plays a crucial role in extensin cross-linking in vitro. Biochem. Insights 8 (S2), 1–13. http://dx.doi.org/10.4137/BCI.S31353.
Chesla, S.E., Selvaraj, P., Zhu, C., 1998. Measuring two-dimensional receptor-ligand binding kinetics by micropipette. Biophys. J. 75, 1553–1572. http://dx.doi.org/10.1016/S0006-3495(98)74074-3.
Cheung, A.Y., 1996. Pollen-pistil interactions during pollen-tube growth. Trends Plant Sci. 1, 45–51. http://dx.doi.org/10.1016/S1360-1385(96)80028-8.
Cheung, A.Y., Zhan, X.Y., Wang, H., Wu, H.M., 1996. Organ-specific and agamous-regulated expression and glycosylation of a pollen tube growth-promoting protein. PNAS 93, 3853–3858. http://dx.doi.org/10.1073/pnas.93.9.3853.
Coimbra, S., Pereira, L.G., 2012. Arabinogalactan proteins in Arabidopsis thaliana pollen development. In: Ciftci, Y.O. (Ed.), Transgenic Plants – Advances and limitations. InTech, Croatia, pp. 329–352 https://doi.org/10.5772/30833.
Cosgrove, D.J., 2005. Growth of the plant cell wall. Nat. Rev. Mol. Cell Biol. 6, 850–861. http://dx.doi.org/10.1038/nrm1746.
Ellis, M., Egelund, J., Schultz, C.J., Bacic, A., 2010. Arabinogalactan-proteins: key regulators at the cell surface? Plant Physiol. 153, 403–419. http://dx.doi.org/10.1104/pp.110.156000.
Fricke, W., Jarvis, M.C., Brett, C.T., 2000. Turgor pressure, membrane tension and the control of exocytosis in higher plants. Plant Cell Environ. 23, 999–1003. http://dx.doi.org/10.1046/j.1365-3040.2000.00616.x.
Gane, A.M., Craik, D., Munro, S.L.A., Howlett, G.J., Clarke, A.E., Bacic, A., 1995. Structural analysis of the carbohydrate moiety of arabinogalactan-proteins from stigmas and styles of *Nicotiana alata*. Carbohydr. Res. 277, 67–85. http://dx.doi.org/10.1016/0008-6215(95)00197-2.
Henderson, W.G., How, M.J., Kennedy, G.R., Mooney, E.F., 1973. The interconversion of aqueous boron species and the interaction of borate with diols: A ^{11}B NMR study. Carbohydr. Res. 28, 1–12. http://dx.doi.org/10.1016/S0008-6215(00)82850-5.
Hepler, P.K., 2005. Calcium: a central regulator of plant growth and development. Plant Cell. 17, 2142–2155. http://dx.doi.org/10.1105/tpc.105.032508.
Hu, H., Brown, P.H., 1994. Localization of boron in cell walls of squash and tobacco and its association with pectin; evidence for a structural role of boron in cell wall. Plant Physiol. 105, 681–689. http://dx.doi.org/10.1104/pp.105.2.681.
Kieliszewski, M.J., 2001. The latest hype on Hyp-O-glycosylation codes. Phytochemistry 57, 319–323. http://dx.doi.org/10.1016/S0031-9422(01)00029-2.
Kieliszewski, M.J., Lamport, D.T.A., Tan, L., Cannon, M.C., 2010. Hydroxyproline-rich glycoproteins: form and function, in: Ulvskov, P. (Ed.), Annual Plant Rev.: Plant Polysaccharides, Biosynthesis, and Bioengineering, vol. 41, Wiley-Blackwell, Oxford.
Kobayashi, M., Ono, K., Matoh, T., 1997. Boron nutrition of cultured tobacco BY-2 cells. II. Characterization of the boron-polysaccharide complex. Plant Cell Physiol. 38, 676–683. http://dx.doi.org/10.1093/oxfordjournals.pcp.a029220.
Lamport, D.T.A., Kieliszewski, M.J., Chen, Y., Cannon, M.C., 2011. Role of the extensin superfamily in primary cell wall architecture. Plant Physiol. 156, 11–19. http://dx.doi.org/10.1104/pp.110.169011.
Lamport, D.T.A., Varnai, P., 2013. Periplasmic arabinogalactan glycoproteins act as a calcium capacitor that regulates plant growth and development. New Phytol. 197, 58–64. http://dx.doi.org/10.1111/nph.12005.
Landau, L.D., Lifschitz, E.M., 1986. Theory of Elasticity. Butterworth-Heinemann, Oxford doi: 10.1016/c2009-0-25521-8.
Loomis, W.D., Durst, R.W., 1991. Boron and cell walls. In: Randall, D.D., Blevins, D.G., Miles, C.D. (Eds.), Curr. Top. Plant Biochem. Physiol., vol. 10, University of Missouri, Columbia, pp. 149–178.
Loomis, W.D., Durst, R.W., 1992. Chemistry and biology of boron. BioFactors 3, 229–239 PMID:1605832.
Mascarenhas, J.P., Machlis, L., 1962. Chemotropic response of *Antirrhinum majus* pollen to calcium. Nature 196, 292–293. http://dx.doi.org/10.1038/196292a0.
Matoh, T., Ishigaki, K.I., Mizutami, M., Matsunaga, W., Takabe, K., 1992. Boron nutrition of cultured tobacco BY-2 cells: I. Requirement for and intracellular localization of boron and selection of cells that tolerate low levels of boron. Plant Cell Physiol. 33, 1135–1141. http://dx.doi.org/10.1093/oxfordjournals.pcp.a078365.
Matoh, T., 1997. Boron in plant cell walls. Plant Soil. 193, 59–70. http://dx.doi.org/10.1023/A:1004207824251.
Merkel, R., Nassoy, P., Leung, A., Ritchie, K., Evans, E., 1999. Energy landscapes of receptor-ligand bonds explored with dynamic force spectroscopy. Nature 397, 50–53. http://dx.doi.org/10.1038/16219.
O'Neill, M.A., Eberhard, S., Albersheim, P., Darvill, A.G., 2001. Requirement of borate cross-linking of cell wall rhamnogalacturonan II for Arabidopsis growth. Science 294, 846–849. http://dx.doi.org/10.1126/science.1062319.
Power, P.P., Woods, W.G., 1997. The chemistry of boron and its speciation in plants. Plant Soil. 193, 1–13. http://dx.doi.org/10.1023/A:1004231922434.
Sachs, L., 1984. Applied Statistics: A handbook of techniques, second ed. Springer-Verlag, New York https://doi.org/10.1007/978-1-4612-5246-7.
Schultz, C.J., Johnson, K.L., Currie, G., Bacic, A., 2000. The classical arabinogalactan protein gene family of Arabidopsis. Plant Cell 12, 1751–1767. http://dx.doi.org/10.1105/tpc.12.9.1751.
Schultz, C.J., Ferguson, K.L., Lahnstein, J., Bacic, A., 2004. Post-translational modification of arabinogalactan-peptides of Arabidopsis thaliana: endoplasmic reticulum and glycosylphosphatidylinositol-anchor signal cleavage sites and hydroxylation of proline. https:doi.org/10.1074/jbc.M407594200. J. Biol. Chem. 279, 45503–45511.
Seifert, G.J., Roberts, K., 2007. The biology of Arabinogalactan proteins. Annu. Rev. Plant Biol. 7, 137–161. http://dx.doi.org/10.1146/annurev.arplant.58.032806.103801.
Serpe, M.D., Nothnagel, E.A., 1995. Fraction and structural characterization of arabinogalactan-proteins from the cell-wall of rose cells. Plant Physiol. 109, 1007–1016. http://dx.doi.org/10.1104/pp.109.3.1007.
Seymour, G.B., Tucker, G., Leach, L., 2004. Cell adhesion molecules in plants and animals. Biotechnol. Genet. Eng. Rev. 21, 123–132. http://dx.doi.org/10.1080/02648725.2004.10648051.
Shi, H., Kim, Y., Guo, Y., Stevenson, B., Zhu, J.-K., 2003. The Arabidopsis SOS5 locus encodes a putative cell surface adhesion protein and is required for normal cell expansion. Plant Cell. 15, 19–32. http://dx.doi.org/10.1105/tpc.007872.
Shpak, E., Barba, E., Leykam, J.F., Kieliszewski, M.J., 2001. Contiguous hydroxyproline residues direct hydroxyproline arabinosylation in *Nicotiana tabacum*. J. Biol. Chem. 276, 11272–11278. http://dx.doi.org/10.1074/jbc.M011323200.
Sundd, P., Zou, X., Goetz, D.J., Tees, D.F.J., 2008. Leukocyte adhesion in capillary-sized, P-selectin-coated micropipettes. Microcirculation 15, 109–122. http://dx.doi.org/10.1080/10739680701412971.
Tajmir-Riahi, H.-A., 1983. Sugar complexes with calcium ion: infrared spectra of crystalline D-glucuronic acid and its calcium complexes. Carbohydr. Res. 122, 241–248. http://dx.doi.org/10.1016/0008-6215(83)88335-9.
Tan, L., Leykam, J., Kieliszewski, M.J., 2003. Glycosylation motifs that direct arabinogalactan addition to arabinogalactan-proteins. Plant Physiol. 132, 1362–1369. http://dx.doi.org/10.1104/pp.103.021766.
Tan, L., Qiu, F., Lamport, D.T.A., Kieliszewski, M.J., 2004. Structure of a hydroxyproline-arabinogalactan polysaccharide from repetitive Ala-Hyp expressed in transgenic *Nicotiana tabacum*. J. Biol. Chem. 279, 13156–13165. http://dx.doi.org/10.1074/jbc.M311864200.
Tan, L., Varnai, P., Lamport, D.T.A., Yuan, C.H., Xu, J.F., Qiu, F., Kieliszewski, M.J., 2010. Plant O-hydroxyproline arabinogalactans are composed of repeating trigalactosyl subunits with short bifurcated sidechains. J. Biol. Chem. 285, 24575–24583. http://dx.doi.org/10.1074/jbc.M109.100149.
Tan, L., Showalter, A.M., Egelund, J., Hernandez-Sanchez, A., Doblin, M.S., Bacic, A., 2012. Arabinogalactan-proteins and the research challenges for these enigmatic plant cell surface proteoglycans. Front. Plant Sci. Article 140. http://dx.doi.org/10.3389/fpls.2012.00140.
Taylor, L.P., Hepler, P.K., 1997. Pollen germination and tube growth. Annu. Rev. Plant Physiol. Plant Mol. Biol. 48, 461–491. http://dx.doi.org/10.1146/annurev.arplant.48.1.461.
Tees, D.F.J., Waugh, R.E., Hammer, D.A., 2001a. A microcantilever device to assess the effect of force on the lifetime of selectin-carbohydrate bonds. Biophys. J. 80, 668–682. http://dx.doi.org/10.1016/S0006-3495(01)76047-X.
Tees, D.F.J., Woodward, J.T., Hammer, D.A., 2001b. Reliability theory for receptor-ligand bond dissociation. J. Chem. Phys. 114, 7483–7496. http://dx.doi.org/10.1063/1.1356030.
Tryfona, T., Lian, H.C., Kotake, T., Kaneko, S., Marsh, J., Ichinose, H., Lovegrove, A., Tsumuraya, Y., Shewry, P.R., Stephens, E., Dupree, P., 2010. Carbohydrate structural analysis of wheat flour arabinogalactan proteins. Carbohydr. Res. 345, 2648–2656. http://dx.doi.org/10.1016/j.carres.2010.09.018.
Tryfona, T., Liang, H.C., Kotake, T., Tsumuraya, Y., Stephens, E., Dupree, P., 2012. Structural characterization of Arabidopsis leaf arabinogalactan polysaccharides. Plant Physiol. 160, 635–666. http://dx.doi.org/10.1104/pp.112.202309.
Zhao, J., Yu, F.L., Liang, S.P., Zhou, C., Yang, H.Y., 2002. Changes of calcium distribution in egg cells, zygotes and two-celled proembryos of rice (*Oryza sativa* L.). Sex. Plant Reprod. 14, 331–337. http://dx.doi.org/10.1007/s00497-002-0127-7.